RSC Advances

PAPER

View Article Online
View Journal | View Issue

Cite this: *RSC Adv.*, 2025, **15**, 7693

Immunocytochemistry response of a hybrid (chitosan-*g*-glycidyl methacrylate)-xanthan scaffold for cell proliferation

Argelia Rosillo-de la Torre,[a] Tonantzi Pérez-Moreno,[b] Iraís A. Quintero-Ortega,[a] Padmavati Sahare,[c] Diego A. Bravo-Alfaro,[c] Héctor E. Martínez-Flores,[d] Friné López-Medina,[e] Ramón Román-Doval,[f] Alejandro Gómez-Sánchez,[f] Sandra Herrera-Perez,[g] Julie E. Gough,[h] Zaira Yunuen García Carvajal,*[i] Cristina Velasquillo*[j] and Gabriel Luna-Barcenas*[c]

Received 10th September 2024
Accepted 18th December 2024

DOI: 10.1039/d4ra06549b

rsc.li/rsc-advances

In the present work, chitosan-glycidyl methacrylate-xanthan ((CTS-*g*-GMA)-X) hydrogel was successfully synthesized by the chemical reaction of a co-polymer of chitosan-*g*-glycidyl methacrylate (CTS-*g*-GMA), under different stoichiometric molar ratios from 1 : 1 to 1 : 4, and xanthan (X). (CTS-*g*-GMA)-X was synthesized by two methods to obtain a hydrogel: an aqueous acid media followed by neutralization and a neutral aqueous media, with an extended reaction time. Human epidermal keratinocytes (HEK) and nerve cells (neuroblastoma × glioma hybrid cell NG108-15) were sown over the hydrogels, and their vitality was determined using a calcein stain. The viability for keratinocytes and nerve cells was quantified using a DNA (proliferation) assay at several intervals. Additionally, immunocytochemistry, detecting E-cadherin, fibronectin, and laminin proteins in HEK, was performed to discard possible diseases caused by (CTS-*g*-GMA)-X hydrogels. The (CTS-GMA) shows greater results compared with the positive control (glass) and the pure chitosan; all polymers show similar satisfactory behaviors between them.

1. Introduction

Due to their abundant availability and unique biological properties, natural polymers have attracted significant interest in regenerative medicine, particularly for applications such as cell scaffolding, wound dressing, tissue regeneration, and wound healing. These materials exhibit vital attributes, including biocompatibility and structures similar to the extracellular matrix (ECM) components. As a result, they have facilitated the development and application of new natural and semi-synthetic materials that mimic the structure and functionality of tissues while also providing favorable conditions for cell growth.[1] For example, designing a cellular scaffold involves tailoring the biomaterial's properties to encourage proper interaction between cells and the ECM, which is crucial for effective tissue formation.[2] Therefore, selecting the appropriate components for the biomaterial is essential. Materials under investigation for these applications include collagen, cellulose, alginate, chitin, hyaluronic acid, starch, and chitosan.

Chitin, the second most abundant polysaccharide in nature after cellulose, is converted into chitosan (CTS), a natural polymer, through deacetylation.[3] Due to its structural similarity to natural glycosaminoglycans and its biodegradability by human enzymes such as lysozyme, CTS has been extensively explored for various tissue engineering applications.[4–6] Furthermore, CTS possesses several attractive properties,

[a]*División de Ciencias e Ingenierías, Universidad de Guanajuato, Guanajuato, Leon, GTO 37150 Mexico. E-mail: rosillo.a@ugto.mx; iraisq@fisica.ugto.mx*

[b]*División de Investigación y Posgrado, Facultad de Ingeniería, Universidad Autónoma de Querétaro, Santiago de Querétaro, QRO 76010, Mexico. E-mail: tonantzi.perez@uaq.mx*

[c]*Tecnologico de Monterrey, Institute of Advanced Materials for Sustainable Manufacturing, Santiago de Queretaro 76130, Mexico. E-mail: padma.sahare@tec.mx; diego.bravo@tec.mx; gabriel.luna@tec.mx*

[d]*Faculty of Chemical Pharmacology, Universidad Michoacana de San Nicolás de Hidalgo, Morelia, MICH 58240, Mexico. E-mail: hedu65@hotmail.com*

[e]*Universidad Autónoma de Tlaxcala, Apizaco, TLAX 90401, Mexico. E-mail: frine.lopez@uatx.mx*

[f]*Tecnológico Nacional de México, Instituto Tecnológico del Valle de Etla, Santiago Suchilquitongo, OAX 68230, Mexico. E-mail: rrdoval.11@gmail.com; drek26@hotmail.com*

[g]*Tecnológico Nacional de México en Celaya, Celaya, Gto. 38010, Mexico. E-mail: sandra.herrera@itcelaya.edu.mx*

[h]*Department of Materials and Henry Royce Institute, The University of Manchester, Manchester M13 9PL, UK. E-mail: j.gough@manchester.ac.uk*

[i]*Biotecnología Médica y Farmacéutica, Centro de Investigación y Asistencia en Tecnología y Diseño del Estado de Jalisco A.C. (CIATEJ), Guadalajara 44270, Jalisco, Mexico. E-mail: zgarcia@ciatej.mx*

[j]*Unidad de Ingeniería de Tejidos, Terapia Celular y Medicina Regenerativa, Instituto Nacional de Rehabilitación Luis Guillermo Ibarra Ibarra, Ciudad de México 14389, CDMX, Mexico. E-mail: mvelasquillo@inr.gob.mx*

including low toxicity, a cationic nature, and versatile preparation methods that allow for producing a wide range of biomaterials (*e.g.*, scaffolds, films, hydrogels, and foams). Its functional groups also enable the functionalization or conjugation of biomolecules, making it highly suitable for tissue engineering.[7] CTS-based hydrogels are widely investigated in skin tissue engineering, with numerous studies demonstrating the *in vitro* proliferation of various cell types, such as fibroblasts and keratinocytes, to form skin layers.[8–12] Additionally, neuronal cell growth has been observed *in vivo* and *in vitro*.[13,14] Moreover, there is strong evidence supporting the acceleration of the wound-healing process when wounds are in direct contact with CTS-based hydrogels, as shown in various *in vivo* models[15–18] and clinical studies.[19]

Xanthan gum (X), an exopolysaccharide produced by the bacterium *Xanthomonas*, is an intriguing biomaterial for various biomedical applications, including tissue engineering and drug delivery, due to its desirable properties such as excellent biocompatibility, biodegradability, non-toxicity, and immunological activity.[20,21] Several studies have focused on evaluating X-based biomaterials to promote the growth and proliferation of specialized cells for skin regeneration.[22,23] However, X-based biomaterials for nerve cell tissue engineering[24–26] have not been as extensively investigated as their chitosan (CTS) counterparts. This study evaluates the *in vitro* biocompatibility of (CTS-*g*-GMA)-X hydrogels as extracellular matrix (ECM) supports (scaffolds) for fibroblasts, keratinocytes, and nerve cells, using assays such as calcein viability, DNA quantification for cell number, peroxide levels, interleukin-1β, and immunocytochemistry.

2. Materials and methods

2.1. Materials

The commercial reagents were from Aldrich Chemical and were used without additional purification. The chitosan had a degree of deacetylation of about 87%, determined by a titration method, and an average molecular weight of 300 kDa, determined by viscometry in a 0.1 M acetic acid and 0.2 M sodium chloride solution at 25 °C. The Mark–Houwink constants, α, and K, were taken from Milas *et al.*[27] for the xanthan (X) and from Kasaai *et al.*[28] for chitosan (CTS). The liquid glycidyl methacrylate (GMA) had 97% purity and was used without additional purification.

2.2. Cells culture

2.2.1. Dermal fibroblasts. The dermal fibroblasts for the primary culture used for the experiments were obtained from the newborn foreskin. Informed consent was obtained from each subject's parents (Hospital Angeles del Pedregal, México). The skin was removed, cleaned in 10 mL of Microcyn® for two minutes, and then maintained in a complete growth medium made up of Dulbecco's modified eagle's medium (DMEM) (Life Technologies Inc. Invitrogen) with 10% fetal bovine serum, 1% penicillin–streptomycin, and 1% amphotericin (Life Technologies Inc. Invitrogen). Explant techniques obtained the fibroblasts. First, the tissue (1–2 g) was minced and incubated in 10 mL of 3% collagenase (Worthington, USA) in DMEM media with 2% penicillin–streptomycin–amphotericin solution for four hours in a shaker at 37 °C. The lysate was centrifuged at 800×*g* for 5 min, and the supernatant was discarded. Next, the cell pellet was washed twice in phosphate buffer saline (PBS) supplemented with a 2% penicillin–streptomycin–amphotericin solution. Aspirate the supernatant, tap the pellet to dissociate the cells, and resuspend them in 1 mL of fresh complete growth medium. The cell pellet was filtered through a nylon mesh of 42 μm and cultured in a single T25 cm^2 flask. The following day, cells were washed twice in 0.9% saline solution to remove red blood cells (RBC). The tissue culture continued with exchange every three days until confluent cell monolayers were formed. After three or four subcultures, homogeneous, slim, spindle-shaped cells growing in characteristic swirls were obtained. Dermal fibroblasts were used for these experiments in their third and fifth passages.[29,30]

2.2.2. Keratinocytes. Human epidermal keratinocytes from adults (HEKa) were proliferated in T75 flasks with a surface treatment to ensure optimal cell attachment and growth in DMEM (5% FBS and 1% antibiotic). H413 keratinocytes were proliferated in T75 flasks with a surface treatment to ensure optimal cell attachment and growth in a DMEM:F12 media supplemented with 50 mL of hydrocortisone per liter of media.[31] Both keratinocytes were maintained at 37 °C in a humidified incubator with 5% CO_2. The keratinocytes used were both from the cell line (H413) and the primary culture (HEKa) to be able to make a comparison between both cell lines and to be able to evaluate the cell viability of the material against both modified and "natural" keratinocytes.

2.2.3. Murine BALB/c monocyte-macrophage cell line J774A.1. The murine BALB/c monocyte-macrophage cell line J774A.1 was obtained from the European Collection of Cell Cultures (no. 91051511). Cells were proliferated in T75 flasks with a surface treatment to ensure optimal cell attachment and growth in a DMEM supplemented with 10% fetal bovine serum (FBS) and 1% antibiotic (all from Life Technologies, Paisley, Scotland). In addition, cells were cultured in Nunc tissue culture flasks and plates (Nunclon, Oxford, UK) and maintained at 37 °C in a humidified incubator with 5% CO_2.[32]

2.2.4. Nerve cells line NG108-15. Nerve cells line NG108-15 were proliferated in T75 flasks with a surface treatment with proprietary Nunclon Delta surface to ensure optimal cell attachment and growth, with DMEM high glucose media without antibiotics, supplemented with 5% FBS, 1% HAT, and 1% of antibiotic, were maintained at 37 °C in a humidified incubator with 5% CO_2.

2.3. (CTS-*g*-GMA)-X hydrogel synthesis

The (CTS-*g*-GMA)-X hydrogels were synthesized by modifying the method proposed by Elizalde-Peña *et al.* 2008.[33] The (CTS-*g*-GMA)-X hydrogels were labeled Z11E, Z12E, Z13E, and Z14E, respectively. The numbers 1 : 1, 1 : 2, 1 : 3, and 1 : 4 correspond to stoichiometric molar ratios of CTS : GMA. E = A for CTS-*g*-GMA materials dissolved in acid solution and E = B for neutral dissolution (Table 1).[33,34]

Table 1 General reaction conditions for the materials Z, for both methods: A acidic and B neutral media

	General conditions			
Material	Stoichiometric ratio (CTS : GMA)	CTS-*g*-GMA solvent	Xanthan solvent	Gravimetric ratio (CTS-*g*-GMA) : X
Z11A	1 : 1	Acetic acid 0.4 M	Distilled water	1 : 1
Z12A	1 : 2			
Z13A	1 : 3			
Z14A	1 : 4			
Z11B	1 : 1	Distilled water		
Z12B	1 : 2			
Z13B	1 : 3			
Z14B	1 : 4			

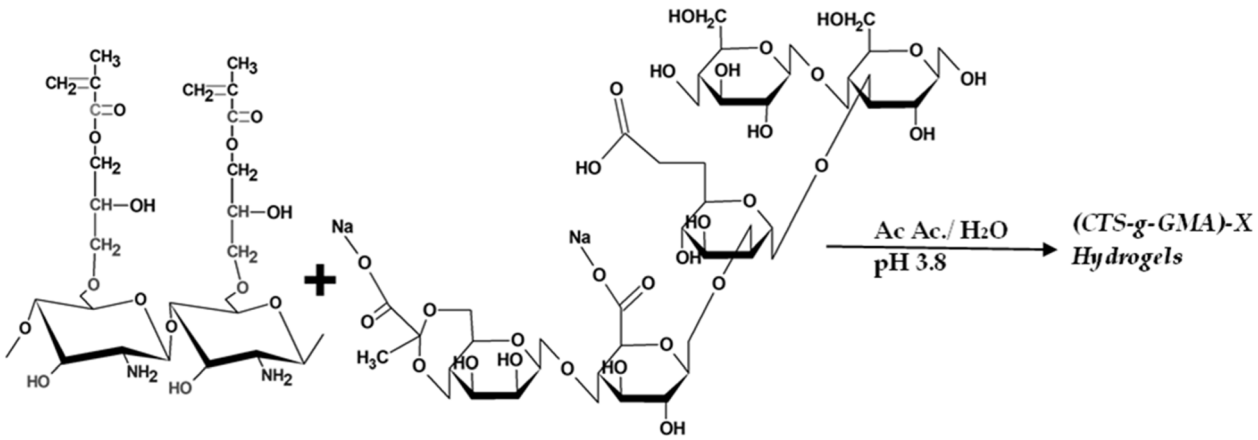

Fig. 1 The proposed chemical reaction for synthesizing the (CTS-*g*-GMA)-X hydrogels.

To obtain a pH similar to physiological, we used a neutral and acid aqueous media to synthesize CTS-*g*-GMA-X hydrogels. In an Erlenmeyer flask, a known quantity, in dry weight, of CTS-*g*-GMA was placed, and then an acetic acid solution of 0.4 M (pH mixture 3.1) was added for series A or distilled water for series B. When the CTS-*g*-GMA was dissolved, the xanthan solution was added slowly. The vial was closed, then a nitrogen flow was introduced; the temperature was 50 ± 1 °C, and constant magnetic agitation was used; the reaction scheme is shown in Fig. 1. The gas flow, heating, and agitation were stopped after one hour (for series A) or four hours (for series B). The product was cooled down in an ice bath for 15 minutes to complete the reaction.

NaOH 0.2 M solution was added for the polymer's series A until a pH of *ca.* 6.8 was reached. Under these conditions, white pearls remained formed, immersed in a colorless solution, and they were recovered by decantation. The pearls were rinsed several times in distilled water to eliminate the residual reactants. The material was recovered by decantation and washed several times in distilled water for the series B polymers to eliminate the residual reactants. Both products were dried in an oven for one hour at 45 °C to obtain films for the subsequent characterization.

All the items used for the tests were conditioned to avoid introducing microbes that could have been picked up while handling the materials in non-sterile places. First, material discs of 10 mm diameter were placed in 48-well plates and were immersed twice in 1 mL of ethanol (70%) for 15 minutes. Then, the ethanol was removed, washed twice with sterile PBS, and maintained overnight in a sterile environment.[33]

2.4. Infrared characterization

Infrared spectroscopy determined the structural differences between both series of materials. The FTIR spectra were recorded on a PerkinElmer spectrometer (model Spectrum One) in the 4000 to 450 cm^{-1} range at a resolution of 4 cm^{-1} in transmission mode.

2.5. Live/dead assay

A LIVE–DEAD® Viability/Cytotoxicity Kit (L-3224, Molecular Probes, Invitrogen) was used to check the cell viability. The cells were seeded at a density of 4×10^4 cells per mL in corresponding media onto each disc of polymer; additionally, glasses were used as a positive control. Each well received 500 mL of calcein AM in PBS containing 2 mM of EthD1, which was added for 20 minutes of incubation. The times for this assay were 1 and 5 days, after which media was removed, and the samples were rinsed three times with PBS. Following removing the media, each sample was placed on a glass microscope slide and observed under a fluorescence microscope; healthy cells fluoresce green, while damaged cells fluoresce red. All assays were made in triplicate.

2.6. DNA assay for cell number

H413 keratinocytes were seeded at a density of 4×10^4 cells per mL in DMEM:F12 onto each polymer; additionally, glass coverslips were used as a positive control. The keratinocyte's behaviors were observed quantitatively on the materials mediated by a DNA assay for cell number. The times for this assay were 1, 3, and 7 days. After this time, the media was removed, and samples were rinsed with PBS. Each sample was transferred to a separate replicate multiwell plate. Distilled water was added to each new well, and samples were freeze-thawed three times. Aliquots of 100 mL of the specimens, standards, and blank (distilled water) were placed into a 96-well plate, and 100 mL of Hoechst stain was added to each well. The plate was shaken for 10 seconds, and fluorescence measurements at 355 nm excitation and 460 nm emission were carried out using a fluorescence plate reader (Fluostar Optima).[35,36] All assays were made in triplicate.

2.7. Interleukin 1b assay (IL-1β)

This assay quantitatively determines the IL-1β in cell culture supernatant released for the macrophages when seeded onto the materials. Cells were cultured for 2 and 48 hours on the material samples.

We used 50 μg mL^{-1} of lipopolysaccharide (LPS) as a positive control for the Il-1β release at various concentrations at both times. The assay was performed, and the optical density of each well was determined using a microplate reader at 450 nm (measurement) and 540 nm (reference) wavelengths.[32] All assays were made in triplicate.

2.8. Immunocytochemistry (ICC)

This test has been made only for the HEKa. Fibronectin, laminin, and E-cadherin antibodies were detected in the cells by ICC protocol, using rabbit IgG as a secondary antibody for fibronectin and laminin; for E-cadherin, mouse IgG and rabbit IgG were used. This assay was performed for 1 and 5 days, respectively, after which media was removed, and the samples were rinsed twice with PBS. The cells were fixed in 3–4% paraformaldehyde in PBS for 15 minutes at room temperature and washed twice using ice-cold PBS. The samples were incubated for 10 minutes with PBS containing 0.25% Triton X-100. Samples were washed in PBS three times for 5 minutes.

Cells were incubated with 1% Bovine Serum Albumin (BSA) in PBS for 30 minutes to block the unspecific binding of the antibodies. Next, the solution was removed, and cells were incubated in the diluted antibody in 1% BSA in PBS in a humidified chamber for 1 hour at room temperature. After that, the solution was removed, and the cells were washed thrice in PBS, 5 minutes for each wash. Next, the HEKa cells were incubated with the secondary antibody corresponding to 1% BSA for 1 hour at room temperature in the dark, and the solution was removed. After that, the samples were washed thrice with PBS for 5 minutes each in the dark. Finally, the cells were mounted in a coverslip with a drop of mounting medium and stored in the dark at 4 °C overnight to be analyzed using a fluorescence microscope. All assays were made in triplicate.

3. Results

3.1. (CTS-*g*-GMA)-X hydrogel synthesis and characterization

Our research group was the first to report synthesizing and characterizing a functionalized CTS-based biomaterial using the synthetic polymer glycidyl methacrylate (GMA). The resulting hybrid hydrogel (CTS/GMA) exhibited superior mechanical properties compared to CTS hydrogels.[34] Subsequently, we provided evidence for synthesizing a (CTS-*g*-GMA)-xanthan (X) hydrogel. Rheological analysis demonstrated that the composite biomaterial exhibited physical hydrogel behavior, while *in vitro* qualitative studies revealed a decrease in cell viability associated with the GMA content.[37] However, *in vivo* studies highlighted the significant potential of this composite biomaterial for treating spinal cord injuries.[25]

In this study, the films obtained after drying had an optimal thickness for infrared characterization. Fig. 2a shows the infrared spectra of the hydrogels (CTS-*g*-GMA)-X (Z) series B,

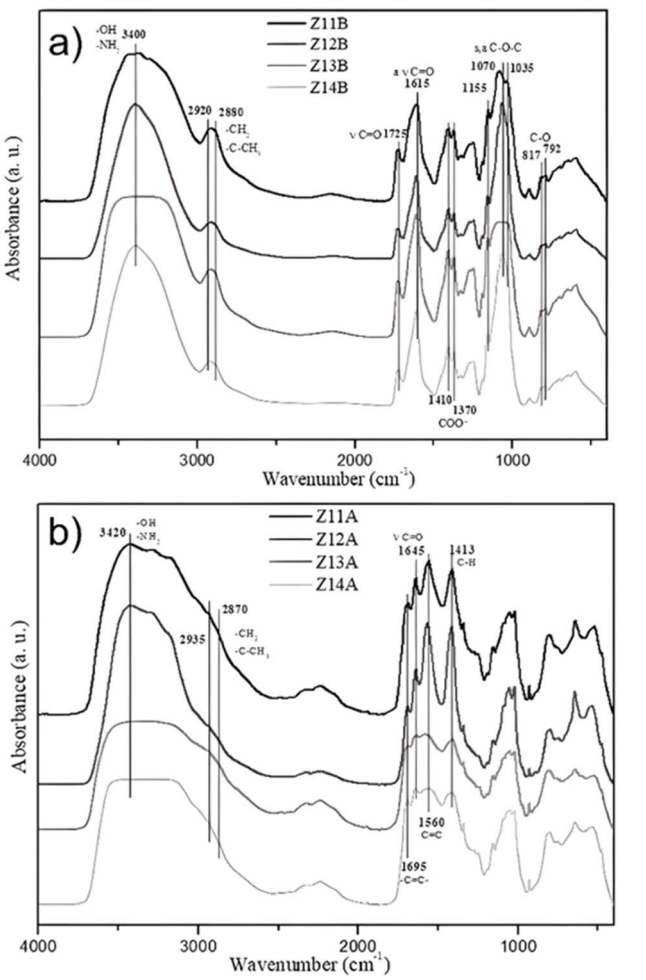

Fig. 2 The infrared spectrum of the (a) hydrogels Z series B. (b) The hydrogels Z series A.

where all spectra display the same bands with minimal changes. For example, it can be observed that in the region corresponding to the OH groups, the Z11B and Z13B samples show wider bands. The band's widening in this region is commonly associated with hydrogen bonding interactions. The OH groups can form hydrogen bonds either with each other or with neighboring water molecules, which causes the band to expand in the FTIR spectrum. This hydrogen bonding is a characteristic phenomenon of materials that contain water or have a high capacity to form hydrogen bonds, such as gels.

Nevertheless, these spectra maintain the characteristic bands compared to the material obtained in an acidic medium without neutralization.[33] However, some differences are evident when comparing series B with series A.

Fig. 2b shows the infrared spectra of series Z A compared to series B. The most notable difference is observed in the bands around 1695 and 1560 cm^{-1}, which correspond to the C=C stretching vibrations of the GMA group attached to chitosan. This result suggests that the chemical treatment used for neutralization slightly degraded the chemical structure of the CTS-*g*-GMA fraction, as reported in previous studies, where it was indicated that the affected groups in CTS-*g*-GMA are the terminal methyl-vinyl groups, which are primarily in contact with the basic medium.[34] In an acid environment, the protonated groups can interact with the epoxy group, decreasing the signals between 1070 and 1035 cm^{-1}, which is associated with the C–O–C group of GMA. This phenomenon correlates with the shift to the left of NH_2 and OH signal compared to Fig. 2a. However, as in series B, the rest of the bands for series A show the same position as the un-neutralized biomaterials described in previous work.[33–36,38,39]

In summary, although no significant differences were found between the spectra of series A and B, the slight degradation observed in the functional groups of GMA suggests that the neutralization treatment influences the chemical structure of the material, especially the groups that react with the basic medium. Finally, the composed biomaterial showed no apparent immune rejection or severe tissue damage; it is necessary to verify the biocompatibility at a cellular level; the scaffold is an exogenous agent that will be interacting with a living host, which could cause different cellular responses, such as inflammatory responses (acute and chronic), foreign body reactions, fibrous capsule development and wound healing responses.[40]

3.2. Epithelial cells

The biocompatibility of a material means that it does not harm cells, allowing them to survive, proliferate, and support tissue formation. To assess the biocompatibility of the (CTS-*g*-GMA)-X hydrogel, we employed calcein, live/dead, and DNA assays with keratinocytes H413 and human epidermal keratinocytes.[41,42] All assays were performed in triplicate, and no significant differences were observed, with a p-value > 0.05.

3.2.1. Live/dead assay. For the live/dead assay in HEKa cells, Fig. 4 shows representative results for 1 and 5 days after cell incubation. The images were obtained using confocal microscopy. Green clusters are visible in both figures, though they appear somewhat undefined. This observation is likely because the polymers support cell growth within their three-dimensional hydrogel structure.

In Fig. 3(a–d), the positive control shows a high number of live cells (green). Meanwhile, all materials exhibit numerous live cells organized into clusters, although some dead cells (red) are also present. In comparison, chitosan shows a more significant proportion of dead cells.

Fig. 3(e–h) presents the live/dead assay results after 5 days of cell inoculation. The glass surface displays a high number of nuclei (dead cells in red) embedded within a layer of cytoplasm (live cells). These nuclei could be due to the high pressure applied to the coverslip. In the CTS group, only remnants of cytoplasm are visible, with no live cells present. The tendency for cells to organize into clusters persists across the biomaterials, though dead cells are evident within these clusters.

3.2.2. DNA assay for counting cells. The viability of H413 keratinocytes was quantified using a DNA (proliferation) assay. Fig. 4 illustrates the growth of keratinocytes on the different processed biomaterials. The results show that some samples (Z14A and Z13B) exhibit behavior similar to the positive control, with cell numbers increasing over time. However, the hydrogels generally maintain better cell viability than the positive control (glass with a treated surface).

For materials in series A, it is noteworthy that there is a peak in cell growth on day 3, followed by a decrease in cell numbers on subsequent days. This growth pattern could be attributed to the chemical structure of the biomaterials, which may create an unfavorable environment for keratinocyte attachment and growth on the material surface. In contrast, the series B polymers support keratinocyte growth at all time points across the biopolymers. This observation could be due to the neutral nature of the reaction, which likely results in a different three-dimensional arrangement in this material, promoting better cell adhesion and proliferation.

The viability of HEKa cells was quantified using the DNA (proliferation) assay. Fig. 5 shows cell growth on the biomaterials. The results indicate that most samples, except for Z13B and Z14B, exhibit better performance than the positive control (glass with a treated surface), with an increase in cell numbers over time. However, while the cell count in Z13B and Z14B is low on day 1, these samples show a significant increase in cell numbers by day 7, with cells doubling in that period.

Likewise in Fig. 5, the samples Z13A and Z14A, containing higher concentrations of GMA, demonstrated increased interactions with CTS through hydroxyl groups. These interactions reduced the availability of amino groups in CTS, which would otherwise interact with X, leading to a notable decrease in the characteristic C=O signals compared to samples with lower GMA concentrations.[37,43] This effect not only limits the availability of positively charged groups but also enhances the exposure and prevalence of negatively charged groups, such as –COOH and –OH, on the surface. The increased density of negative surface charges provides potential chelation sites for positively charged ions or enzymes, thereby modifying the local biochemical environment.[44,45] These surface modifications can negatively affect cell viability, as observed in primary keratocytes HEKa.[46,47]

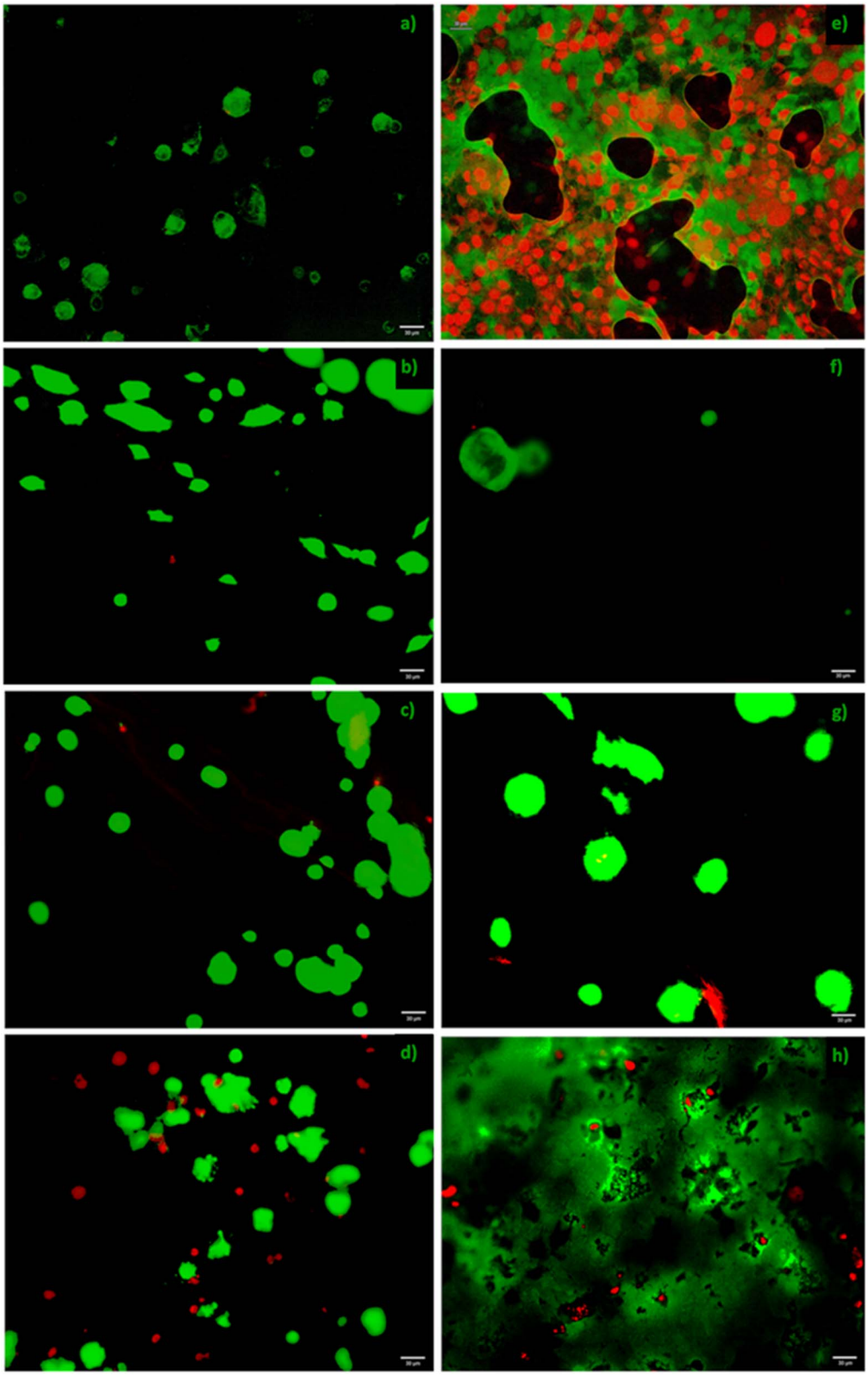

Fig. 3 Confocal microscopy of live/dead assay results: (a) glass (positive control), (b) treatment Z11A, (c) treatment Z12B, and (d) chitosan after 1 day of cell incubation; (e) glass (positive control), (f) treatment Z13A, (g) treatment Z14B, and (h) chitosan after 5 days of cell incubation.

Polymers from series A generally perform better than those from series B, with Z11A showing the most significant growth after seven days. These findings contrast with results obtained for H413 keratinocytes in previous work,[33] where series B demonstrated better attachment and growth. This difference may be attributed to the distinct nature of the two cell types. The

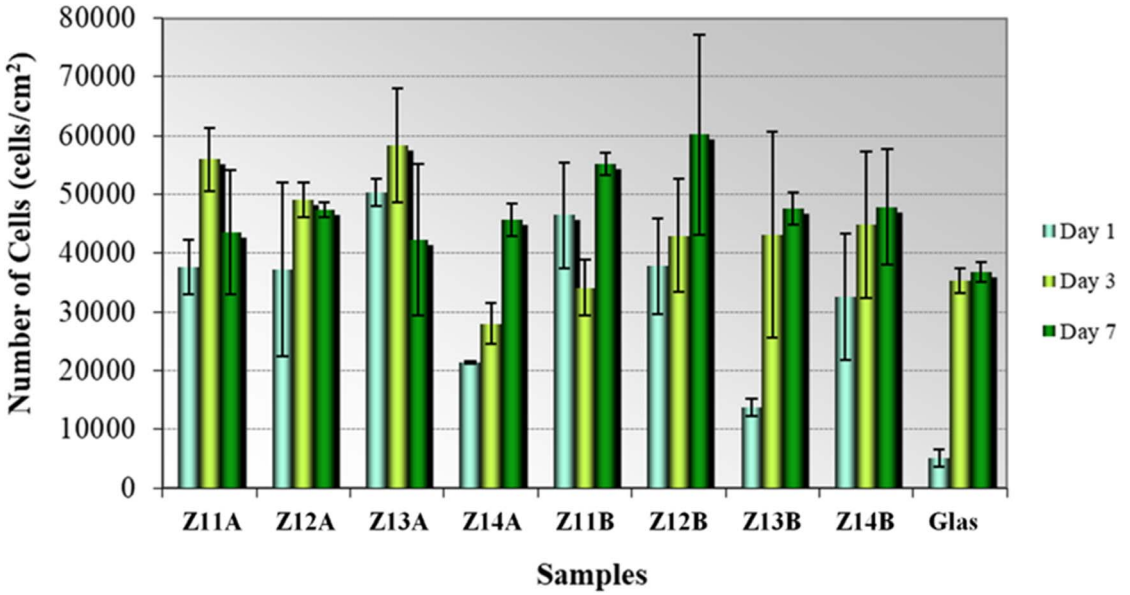

Fig. 4 Cell growth of keratinocytes lines H413 onto polymers and glass (positive control). All assays were made in triplicate; there are no significant differences, with a $p > 0.05$.

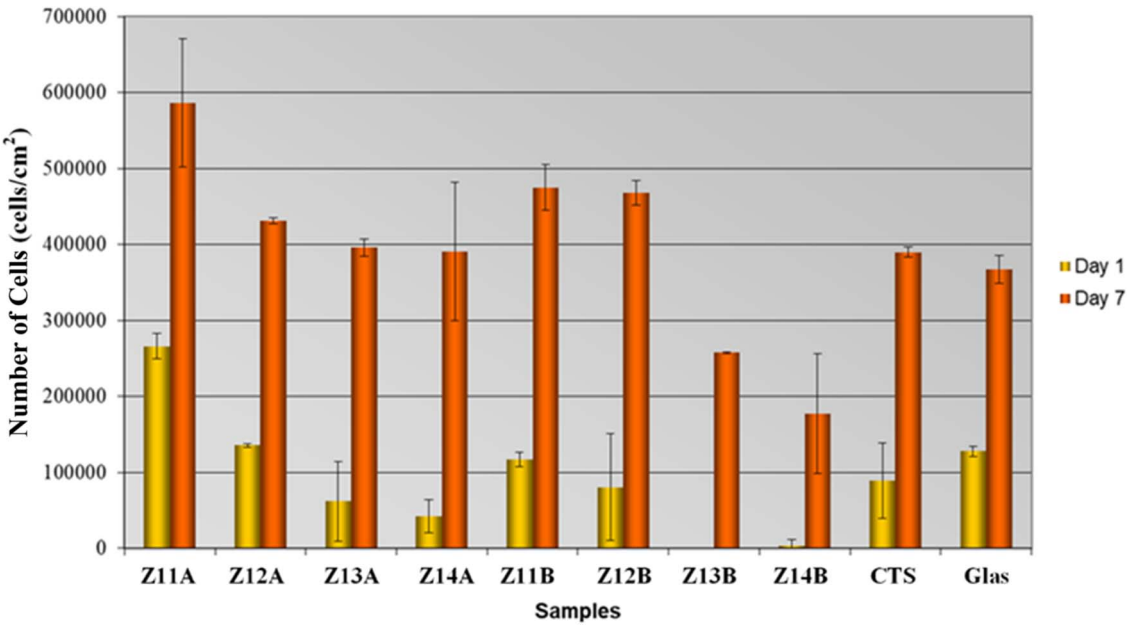

Fig. 5 Cell growth of human epidermal keratinocytes onto polymers, chitosan (precursor), and glass (positive control). From day 1 to day 7, there is significant cell growth in the biomaterials of the present work. All assays were made in triplicate; there are no significant differences, with a $p > 0.05$.

results show no significant differences between most polymers, though notable differences were observed between specific samples on days 1 and 7.

3.2.3. Interleukin 1β assay (IL-1β). For the IL-1β assay, eight points were analyzed to construct the calibration curve using the recombinant mouse IL-1β standard. Fig. 6 presents a comparative histogram of the values obtained in the test. This graph shows a low concentration of IL-1β after 2 hours of incubation, with values similar to the positive control. However, after 48 hours, an increase in IL-1β levels was observed in response to Z13A, which exhibited the highest value, approximately 300 pg mL^{-1}.

In contrast, the remaining samples had values below 200 pg mL^{-1}, with chitosan showing low activity and yielding the lowest value compared to the positive control.

All samples responded similarly when in contact with macrophages, although their values were generally higher than those reported by other studies. Our samples were used at 1 mg mL^{-1},

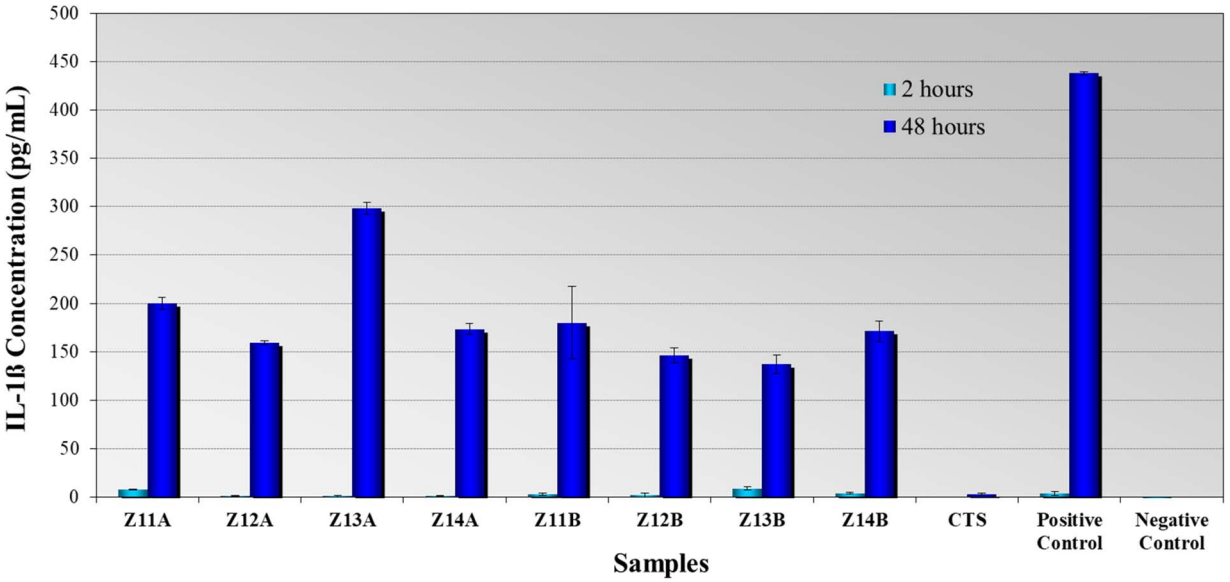

Fig. 6 Interleukin-1β production by mouse macrophages J774A.1 after 2 and 48 hours. All assays were made in triplicate; there are no significant differences, with a $p > 0.05$.

whereas other studies employed concentrations of 50 or 500 mg mL^{-1} for incubation periods of 18 or 24 hours (Table 2).[48–50] The observed increase in IL-1β production may be attributed to the expected behavior of macrophages in the presence of foreign materials, triggering a non-specific inflammatory response that could promote accelerated biodegradation.

3.2.4. SEM. Fig. 7 presents scanning electron microscopy (SEM) images obtained in secondary electron mode. Panel 7a shows the polymer surface with macrophages attached. The polymer thickness was measured at approximately 4 μm, while the macrophage diameter was around 10 μm. Meanwhile, the image in Fig. 7c illustrates signs of material degradation, likely due to macrophage resorption of the surface. Although no significant degradation was observed in the images, some macrophages displayed a spread morphology (Fig. 7b and d). This observation suggests that the macrophages may be involved in the degradation of the polymer. Given their ability to support cell viability, the materials induced only a mild inflammatory response and could be proposed as potential scaffolds for tissue engineering applications.

Table 2 Concentrations and values of IL-1b of different polymers based on chitosan compared with the materials

Material	Dose (μg ml^{-1})	Incubation time (h)	IL-1β production (pg ml^{-1})	Ref.
Oligochitosan	40	18	101.9 ± 46.6	49
S-DAC70	50	24	28	50
S-DAC70	500	24	45	50
Chitosan–DNA[a]	—	24	No detected	51
Z13A	1000	48	298.5 ± 6.1	—
CTS 0.5%	1000	48	3.2 ± 0.5	—

[a] With 0.1, 1, 10, and 20 μg of DNA.

3.3. Immunocytochemistry (ICC)

Cell adhesion is a critical cell proliferation process involving several multi-protein complexes. E-Cadherin (epithelial) is a crucial cell–cell adhesion molecule in epithelial tissues, playing an essential role in forming and maintaining these tissues' typical architecture and function.[51]

Fibronectin is one of the most studied matrix glycoproteins, owing to its crucial role in the adhesion of various cell types. It is vital for regulating cell behavior through communication with intracellular and extracellular environments and is essential in wound healing.[52,53] Laminin, the most abundant structural multidomain protein in basement membranes, regulates cell attachment, proliferation, differentiation, and motility.

Additionally, it promotes neurite regeneration, highlighting its multifunctionality.[54–56] Cellular responses such as adhesion, spreading, proliferation, and differentiation are influenced by proteins at the cell–biomaterial interface. These proteins' proper expression and function—such as E-cadherin, fibronectin, and laminin—are essential for promoting favorable cellular responses. In contrast, dysfunctional or improperly expressed proteins have been linked to immune reactions, carcinogenic phenotypes, and dystrophies.[57–61] Therefore, evaluating the behavior of these proteins when a biomaterial is exposed to the host is crucial.

3.3.1. E-Cadherin antibody. Fig. 8a–d show representative results for the E-cadherin antibody; after 5 days of cell incubation, confocal microscopy obtained the behavior of most polymers as a correct stain without abnormal signals such as excess or lack of this protein. In addition, the nuclei stain (blue) can be appreciated. Still, it did not show apparent alterations, which indicates that the polymers did not affect the correct union between this type of cell.

3.3.2. Fibronectin antibody. Fig. 8e–h show representative results for fibronectin staining after 5 days of cell incubation, obtained using confocal microscopy. Although the fluorescence

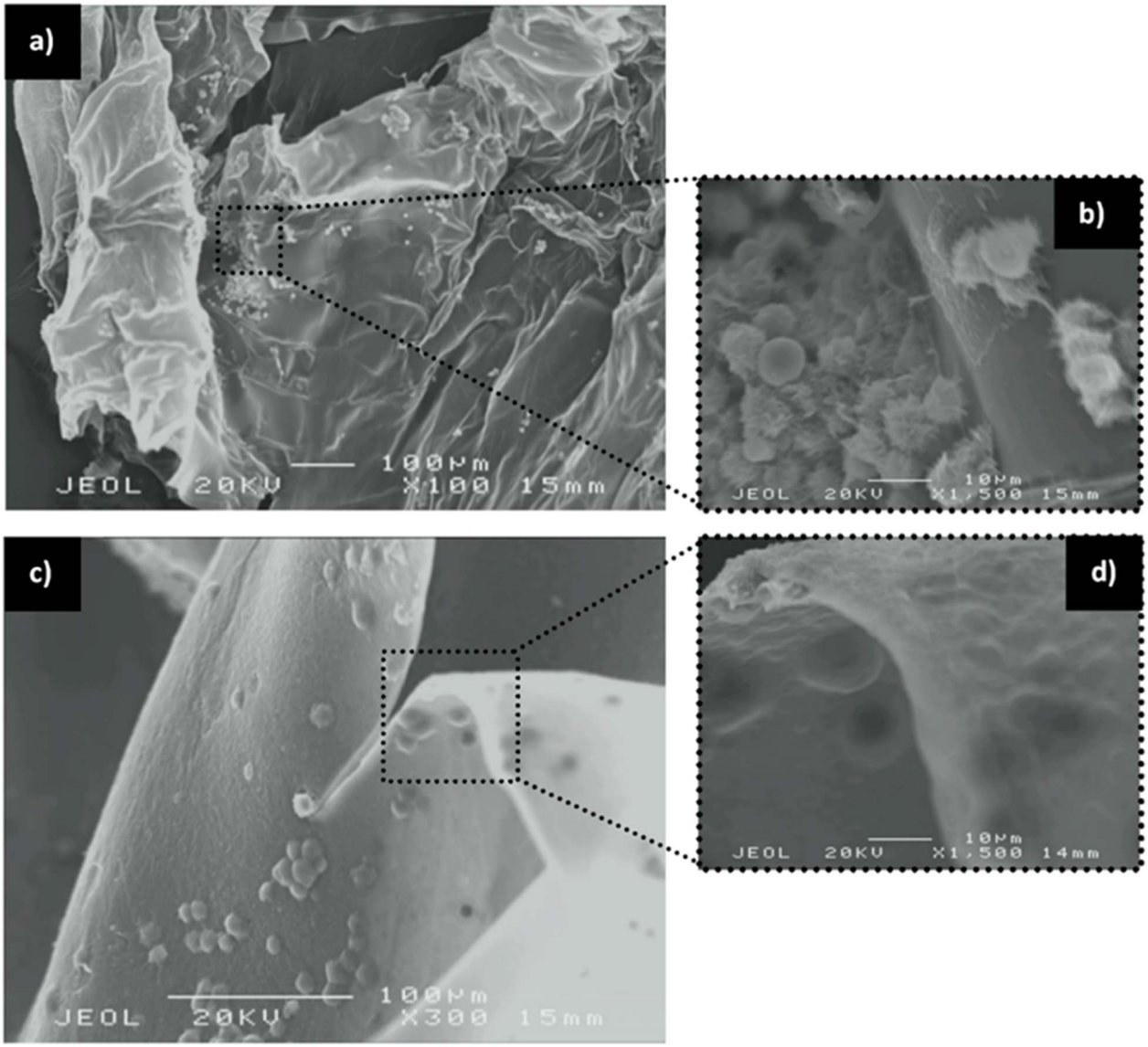

Fig. 7 Micrographs showing polymer degradation around macrophage (a and b), and without degradation and an inactive macrophage (c and d).

intensity is relatively low, these images reveal proper fibronectin staining. When comparing the polymers to the positive control (glass), it can be concluded that the polymers do not inhibit fibronectin production, allowing the cells to carry out their normal functions.

3.3.3. Laminin antibody. Fig. 8i–l show the results for the laminin antibody after 5 days of cell culture, and images were obtained by confocal microscopy. As in the previous antibody results for E-cadherin and fibronectin, the stain for the laminin antibody is appropriate since keratinocytes did not show alterations or abnormal behavior for most of the polymers. Consequently, a direct comparison with the positive control glass can be made.

3.4. Nerve cells (NG108-15)

3.4.1. DNA assay for counting cells. Fig. 9 shows cell growth on the biomaterials. The results indicate that most samples exhibit lower growth than the positive control (glass with a treated surface).

While no significant differences were observed between most of the polymers, notable differences were found between some samples on days 1 and 7, particularly in the positive control. Although cell growth was lower than in the control specimens, there is sufficient evidence to support the viability of this type of cell for growth on the biomaterials.

3.4.2. Live/dead assay. Fig. 10 shows the live/dead assay results after 5 days of the cell inoculation; the glass shows several nuclei (dead cells) in red, immersed in a layer of live cells.

The trend continues to organize the cells in straight clusters with a random orientation on the biomaterials. However, in all the polymers, including chitosan film, it is evident that dead cells are absent in these clusters. This observation could be attributed to the lack of attachment of dead cells and their possible discard in some of the washes, especially when DNA

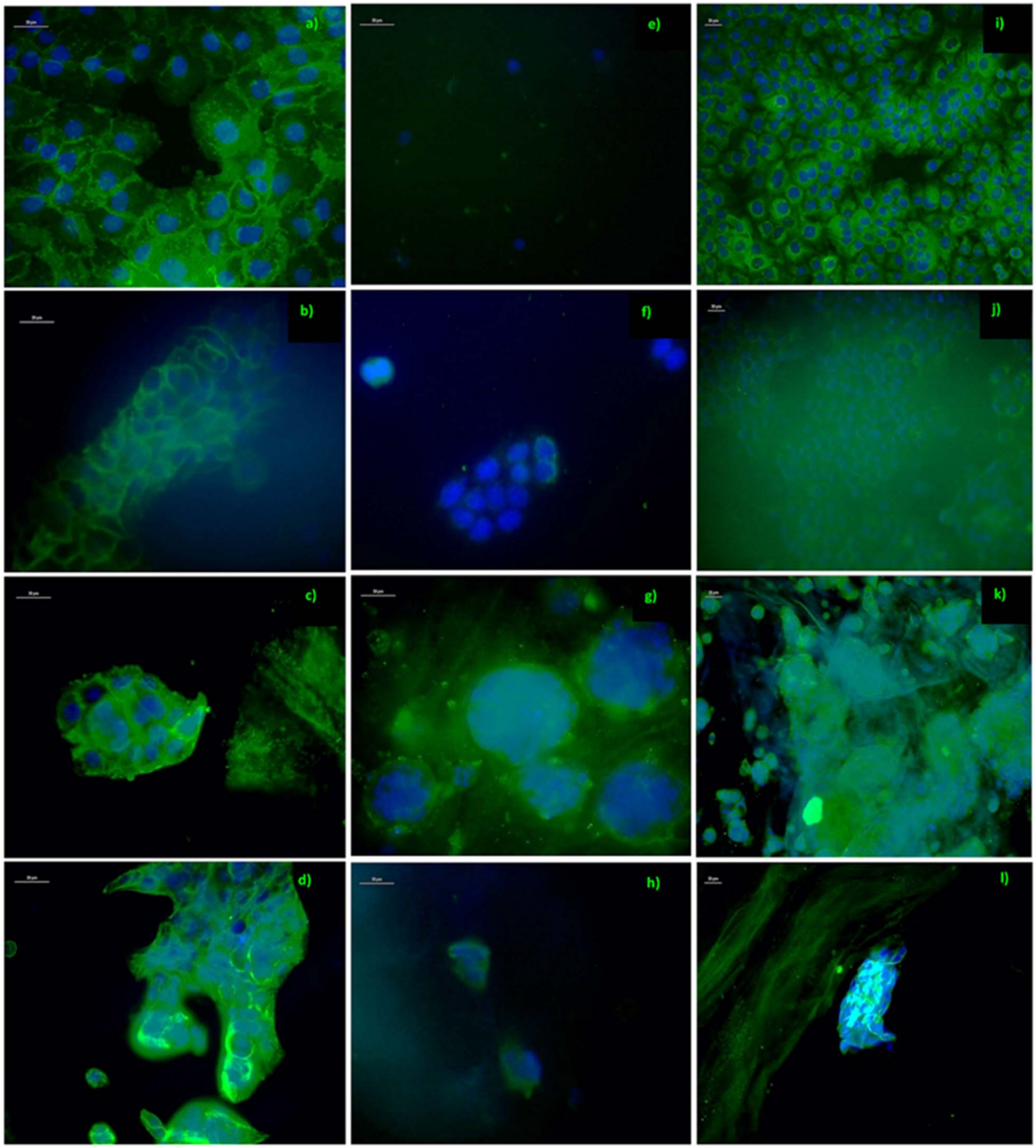

Fig. 8 Representative images for E-cadherin antibody stain on (a) glass (positive control), (b) chitosan, (c) Z12B, and (d) Z11A, fibronectin antibody stain on (e) glass (positive control), (f) chitosan, (g) Z12B, and (h) Z14B and laminin antibody stain on (i) glass (positive control), (j) chitosan, (k) Z11B, and (l) Z14A after 5 days of incubation. The blue regions are the cells' nuclei.

assay shows a low number of cells onto biomaterials compared with the glass.

3.4.3. SEM. Fig. 11 shows the SEM images of nerve cells NG108-15, after seven days of inoculation, in two different magnifications, 750× and 2000×.

In both cases, it is possible to observe the attachment to the surface of the polymers, and the cells present a habitual behavior and a web-like morphology. These images confirm the random orientation and the straight cluster formation observed in the live/dead assay. In addition, the morphology shown by the cells in the polymers demonstrates that, although the number of cells is low according to DNA assay, the cells are in a suitable environment for their growth and proliferation.

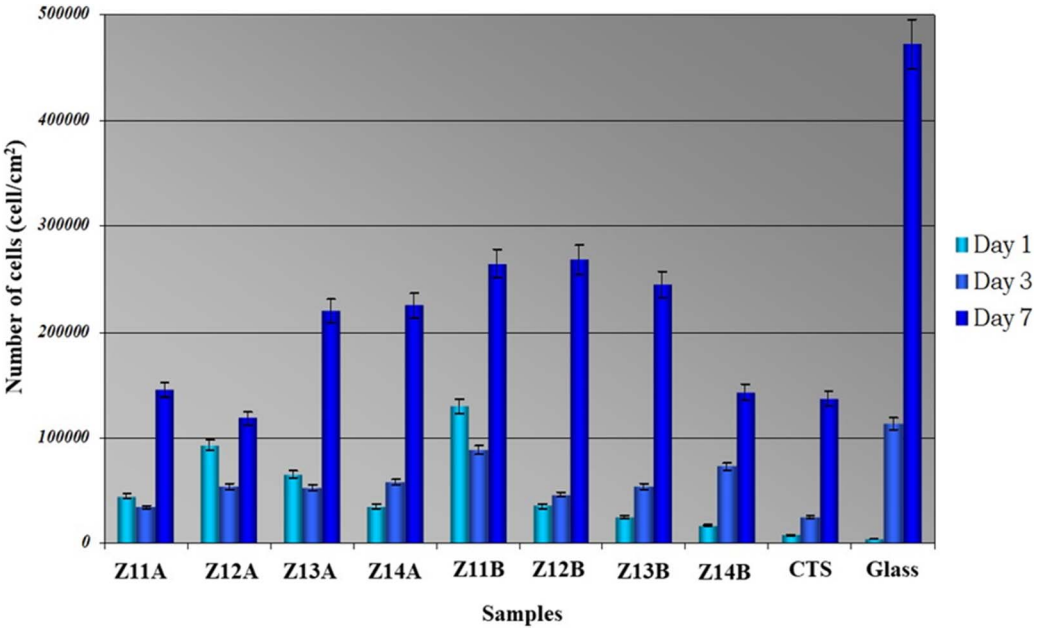

Fig. 9 Cell growth of nerve cells NG108-15 onto biomaterials, chitosan (precursor), and glass (positive control). Cell growth continues in this assay from day 1 to day 7. All assays were made in triplicate; there are no significant differences, with a $p > 0.05$.

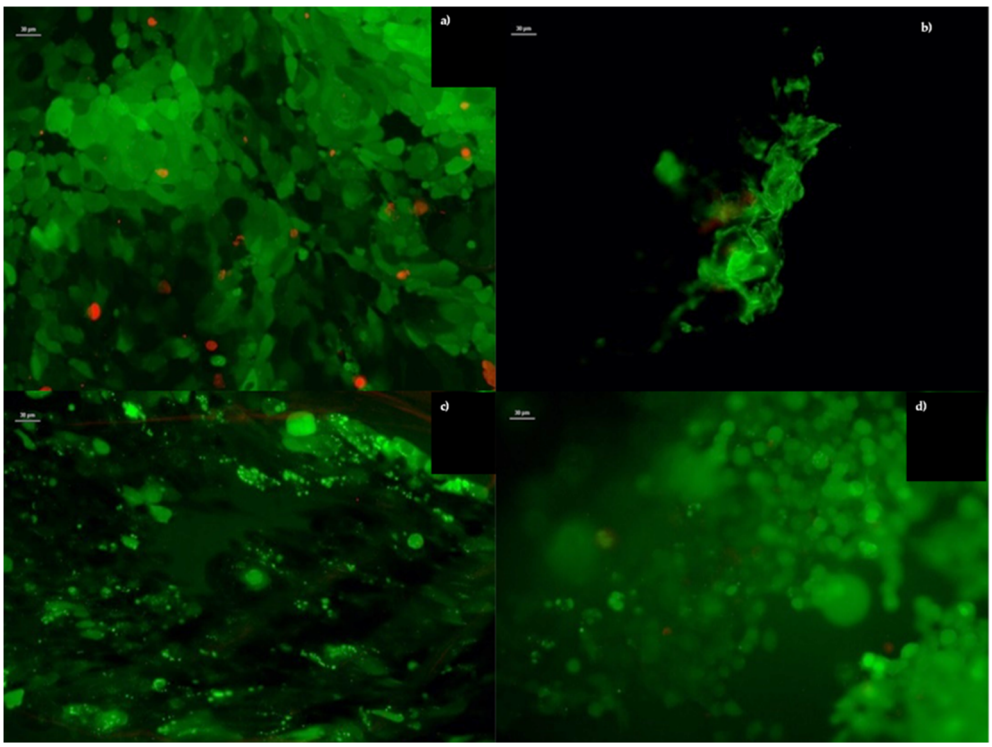

Fig. 10 Representative results for live/dead assay after 5 days of cell incubation, (a) glass (positive control), (b) chitosan, (c) Z11B, and (d) Z14A. Original magnification 20×. Green fluorescent regions denote cell activity, whereas red regions denote null cell activity.

4. Discussion

Due to the ionic nature of the polymers, the reaction mechanism suggests an interaction between the carboxyl group of xanthan and the amino group of chitosan. Adding glycidyl methacrylate to chitosan does not appear to interact with xanthan, as infrared signals show no significant shifts in form or intensity. Based on the FTIR spectra, no significant difference

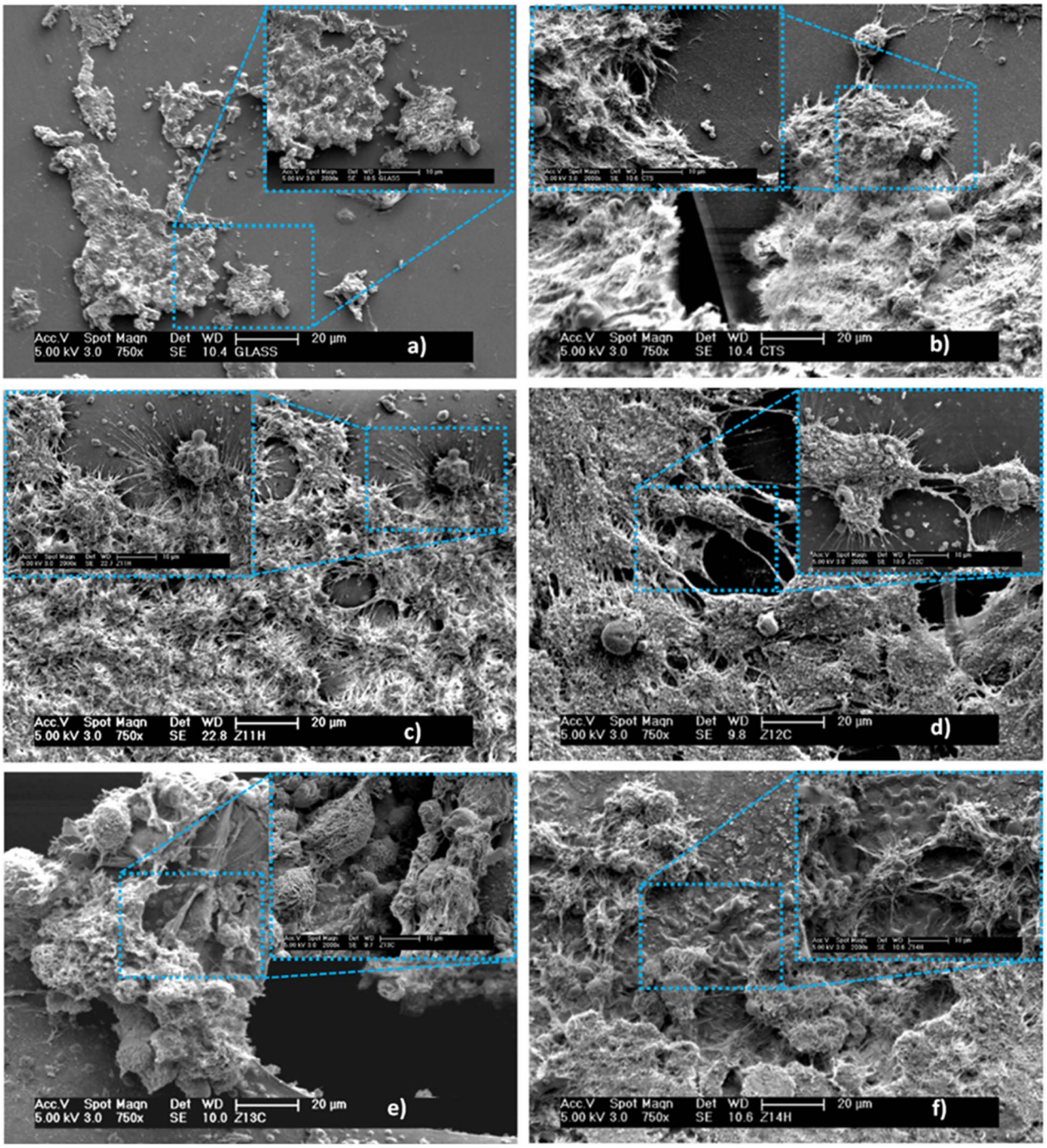

Fig. 11 Micrographs of nerve cells NG108-15 onto (a) glass, (b) chitosan, (c) Z11B, (d) Z12A, (e) Z13A, and (f) Z14B after seven days of cell culture, original magnification 750× and 2000×. The growth of cell colonies denotes that the biomaterials are an excellent scaffold for cell growth. These series of biomaterials have been tagged as Z11, 12, 13, and 14 are stoichiometric ratios for (CTS-*g*-GMA), (A) chemically modified, and (B) aqueous media.

was observed between the two methods, indicating that the materials can be used in cell culture without affecting the pH of the culture media.

The results from the peroxide assay show that these materials do not provoke a substantial reaction in macrophages over short periods (6 hours), unlike the negative control (copper), which exhibited higher values than the polymers. These findings support that the material does not induce an immune response, allowing cell protection and growth on the biomaterial surface. However, the IL-1β assay reveals that the A series polymers promote an increase in the inflammatory response after 48 hours, while the B series materials do not. In the context of biomedical applications, this low inflammatory response enhances the potential for using these materials.

Calcein staining demonstrates an increase in the viability of human fibroblasts. The DNA assay results indicate that the materials have potential as scaffolds for H413 keratinocytes, as cell viability was maintained for 7 days in culture, with a high cell density (many cells per mL). These findings support using these materials in the biomedical field as scaffolds, given their ability to maintain cell viability in connective, skin, and nerve tissue.

The DNA assay for human epidermal keratinocytes shows strong cell preservation and growth in most samples, with results comparable to the blank (glass with a treated surface). Immunocytochemistry staining revealed good labeling for all antibodies tested in this study with human epidermal keratinocytes, and the results were comparable to the positive control (glass). These polymers do not negatively affect the growth and proliferation of this cell type. Additionally, live/dead, SEM, and DNA assays on NG108-15 nerve cells showed good viability, with a significant proportion of cells remaining active after 7 days.

Given the importance of laminin in promoting neurite regeneration, this result is crucial, as this study aims to regenerate spinal cord channels. If the laminin antibody staining is accurate for this cell type on our biomaterials, we can expect similar behavior in nerve cells, as reported in previous studies.[62] Furthermore, the viability of dermal fibroblasts and keratinocytes aligns with the findings of López-Muñoz *et al.*, who demonstrated that CTS-*g*-GMA materials with gold nanoparticles and type I collagen can promote effective skin wound healing.[63]

One of the main limitations of the present study is that, due to the use of membranes and the extended duration of the tests, we were unable to assess the viability of other cell types, which could expand the potential applications of our polymer. For future work, we propose differentiating NG108 cells to evaluate their application in model organisms, such as rats, to scale up to more complex organisms with advanced DNA structures.

In the present work, we have developed a simple yet effective synthesis of a material with good mechanical properties and cell viability for skin and nerve cells, complementing previous studies.[62,63] This type of CTS-*g*-GMA composite supports the proper growth of various cell types and aids in protecting damaged areas. Our material offers a more straightforward and versatile synthesis than other materials, such as fiber matrices. However, its properties are currently more suited to wound care and surface treatments.[64–67] That said, the material we developed demonstrates considerable versatility, as it can be modified to suit specific applications depending on the molecules with which it is functionalized, thus significantly expanding its potential applications.[25,33,34,37,62,63]

5. Conclusions

The present study aimed to synthesize and evaluate the biopolymer CTS-*g*-GMA-X, which maintains a physiological pH close to 7. No significant differences were observed between the two synthesis methods based on FTIR analysis, and neither method negatively affected cell viability, suggesting that these materials may be suitable for biomedical applications. However, whether they are biocompatible *in vivo* and effective for specific medical applications (*e.g.*, skin graft devices) remains to be determined. Nevertheless, the results obtained in this study are promising and strongly support the potential use of these hydrogels as scaffolds for tissue engineering and the repair of spinal cord injuries.

Data availability

The data presented in this article, including the descriptions and information related to , Fig. 4–6 and 9, as well as the ethics committee approval letter for the conducted studies, are available in the Science Data Bank repository at **https://www.scidb.cn/en/anonymous/ZkVGejZq**, with DOI: **https://doi.org/10.57760/sciencedb.19980**.

Author contributions

A. R. T.: investigation, methodology, writing – original draft. T. P. M.: investigation, writing – review & editing. I. A. Q. O.: investigation, methodology, software. P. S.: data curation, writing – original draft, formal analysis. D. A. B. A.: writing – original draft, data curation, software. H. M. F.: conceptualization, methodology. F. L. M.: investigation, software. R. R. D.: formal analysis, visualization, writing – review & editing. A. G. S.: methodology, software, writing – review & editing. S. H. P.: funding acquisition, visualization, investigation. J. E. G.: methodology, validation, supervision. Z. Y. G. C.: conceptualization, formal analysis, resources, supervision. C. V.: validation, funding acquisition, formal analysis, writing – original draft. G. L. B.: conceptualization, funding acquisition, supervision, writing – review & editing.

Conflicts of interest

There are no conflicts to declare.

Acknowledgements

We appreciate access to LIDTRA facilities through its projects: LN295261, LN254119, and LN299082. We also thank M. C. Reyna Araceli Mauricio Sanchez for technical assistance in the FTIR measurements.

Notes and references

1 S. Stratton, N. B. Shelke, K. Hoshino, S. Rudraiah and S. G. Kumbar, Bioactive Polymeric Scaffolds for Tissue Engineering, *Bioact. Mater.*, 2016, **1**, 93–108.
2 M. Jafari, Z. Paknejad, M. R. Rad, S. R. Motamedian, M. J. Eghbal, N. Nadjmi and A. Khojasteh, Polymeric Scaffolds in Tissue Engineering: A Literature Review, *J. Biomed. Mater. Res., Part B*, 2017, **105**, 431–459.
3 G. A. F. Roberts, *Chitin Chemistry*, Macmillan Education UK, 1992.
4 M. M. Islam, M. Shahruzzaman, S. Biswas, M. Nurus Sakib and T. U. Rashid, Chitosan Based Bioactive Materials in

Tissue Engineering Applications-A Review, *Bioact. Mater.*, 2020, **5**, 164–183.

5 S. Kim, Z. K. Cui, B. Koo, J. Zheng, T. Aghaloo and M. Lee, Chitosan-Lysozyme Conjugates for Enzyme-Triggered Hydrogel Degradation in Tissue Engineering Applications, *ACS Appl. Mater. Interfaces*, 2018, **10**, 41138–41145.

6 A. Lončarević, M. Ivanković and A. Rogina, Lysozyme-Induced Degradation of Chitosan: The Characterisation of Degraded Chitosan Scaffolds, *Journal of Tissue Repair and Regeneration*, 2017, **1**, 12–22.

7 S. M. Ahsan, M. Thomas, K. K. Reddy, S. G. Sooraparaju, A. Asthana and I. Bhatnagar, Chitosan as Biomaterial in Drug Delivery and Tissue Engineering, *Int. J. Biol. Macromol.*, 2018, **110**, 97–109.

8 G. I. Howling, P. W. Dettmar, P. A. Goddard, F. C. Hampson, M. Dornish and E. J. Wood, The Effect of Chitin and Chitosan on the Proliferation of Human Skin Fibroblasts and Keratinocytes *in Vitro*, *Biomaterials*, 2001, **22**, 2959–2966.

9 V. Vivcharenko, M. Wojcik and A. Przekora, Cellular Response to Vitamin C-Enriched Chitosan/Agarose Film with Potential Application as Artificial Skin Substitute for Chronic Wound Treatment, *Cells*, 2020, **9**, 1185.

10 P. Makvandi, G. W. Ali, F. della Sala, W. I. Abdel-Fattah and A. Borzacchiello, Biosynthesis and Characterization of Antibac-terial Thermosensitive Hydrogels Based on Corn Silk Extract, Hyaluronic Acid and Nanosilver for Potential Wound Healing, *Carbohydr. Polym.*, 2019, **223**, 115023.

11 H. Xu, S. Huang, J. Wang, Y. Lan, L. Feng, M. Zhu, Y. Xiao, B. Cheng, W. Xue and R. Guo, Enhanced Cutaneous Wound Healing by Functional Injectable Thermo-Sensitive Chitosan-Based Hydrogel Encapsulated Human Umbilical Cord-Mesenchymal Stem Cells, *Int. J. Biol. Macromol.*, 2019, **137**, 433–441.

12 A. M. Heimbuck, T. R. Priddy-Arrington, M. L. Padgett, C. B. Llamas, H. H. Barnett, B. A. Bunnell and M. E. Caldorera-Moore, Development of Responsive Chitosan-Genipin Hydrogels for the Treatment of Wounds, *ACS Appl. Bio Mater.*, 2019, **2**, 2879–2888.

13 F. Yan, M. Li, H. Q. Zhang, G. L. Li, Y. Hua, Y. Shen, X. M. Ji, C. J. Wu, H. An and M. Ren, Collagen-Chitosan Scaffold Impregnated with Bone Marrow Mesenchymal Stem Cells for Treatment of Traumatic Brain Injury, *Neural Regener. Res.*, 2019, **14**, 1780–1786.

14 M. Mattotti, Z. Alvarez, L. Delgado, M. A. Mateos-Timoneda, C. Aparicio, J. A. Planell, S. Alcántara and E. Engel, Differential Neuronal and Glial Behavior on Flat and Micro Patterned Chitosan Films, *Colloids Surf., B*, 2017, **158**, 569–577.

15 C. Intini, L. Elviri, J. Cabral, S. Mros, C. Bergonzi, A. Bianchera, L. Flammini, P. Govoni, E. Barocelli and R. Bettini, 3D-Printed Chitosan-Based Scaffolds: An *in Vitro* Study of Human Skin Cell Growth and an *in Vivo* Wound Healing Evaluation in Experimental Diabetes in Rats, *Carbohydr. Polym.*, 2018, **199**, 593–602.

16 V. Lopes Rocha Correa, J. Assis Martins, T. Ribeiro de Souza, G. de Castro Nunes Rincon, M. Pacheco Miguel, L. Borges de Menezes and A. Correa Amaral, Melatonin Loaded Lecithin–Chitosan Nanoparticles Improved the Wound Healing in Diabetic Rats, *Int. J. Biol. Macromol.*, 2020, **162**, 1465–1475.

17 Z. Aliakbar Ahovan, S. Khosravimelal, B. S. Eftekhari, S. Mehrabi, A. Hashemi, S. Eftekhari, P. Brouki Milan, M. Mobaraki, A. M. Seifalian and M. Gholipourmalekabadi, Thermo-Responsive Chitosan Hydrogel for Healing of Full-Thickness Wounds Infected with XDR Bacteria Isolated from Burn Patients: *In Vitro* and *In Vivo* Animal Model, *Int. J. Biol. Macromol.*, 2020, **164**, 4475–4486.

18 N. Masood, R. Ahmed, M. Tariq, Z. Ahmed, M. S. Masoud, I. Ali, R. Asghar, A. Andleeb and A. Hasan, Silver Nanoparticle Impregnated Chitosan-PEG Hydrogel Enhances Wound Healing in Diabetes Induced Rabbits, *Int. J. Pharm.*, 2019, **559**, 23–36.

19 G. Kratz, M. Back, C. Arnander and O. Larm, Immobilised Heparin Accelerates the Healing of Human Wounds *in Vivo*, *Scand. J. Plast. ReConstr. Surg. Hand Surg.*, 1998, **32**, 381–386.

20 G. Singhvi, N. Hans, N. Shiva and S. Kumar Dubey, Xanthan Gum in Drug Delivery Applications, *In Natural Polysaccharides in Drug Delivery and Biomedical Applications*, 2019, pp. 121–144.

21 A. Kumar, K. M. Rao and S. S. Han, Application of Xanthan Gum as Polysaccharide in Tissue Engineering: A Review, *Carbohydr. Polym.*, 2018, **180**, 128–144.

22 M. Z. Bellini, A. L. R. Pires, M. O. Vasconcelos and A. M. Moraes, Comparison of the Properties of Compacted and Porous La-mellar Chitosan-Xanthan Membranes as Dressings and Scaffolds for the Treatment of Skin Lesions, *J. Appl. Polym. Sci.*, 2012, **125**, E421–E431.

23 A. Alves, S. P. Miguel, A. R. T. S. Araujo, M. J. de Jesus Valle, A. S. Navarro, I. J. Correia, M. P. Ribeiro and P. Coutinho, Xanthan Gum-Konjac Glucomannan Blend Hydrogel for Wound Healing, *Polymers*, 2020, **12**, 99.

24 T. Glaser, V. B. Bueno, D. R. Cornejo, D. F. S. Petri and H. Ulrich, Neuronal Adhesion, Proliferation and Differentiation of Embryonic Stem Cells on Hybrid Scaffolds Made of Xanthan and Magnetite Nanoparticles, *Biomed. Mater.*, 2015, **10**, 045002.

25 D. G. Zarate-Triviño, H. Pool, H. Vergara-Castañeda, E. A. Elizalde-Peña, V. Vallejo-Becerra, F. Villaseñor, E. Prokhorov, J. Gough, B. Garcia-Gaitan and G. Luna-Barcenas, (Chitosan-*g*-Glycidyl Methacrylate)-Collagen II Scaffold for Cartilage Re-generation, *Int. J. Polym. Mater.*, 2020, **69**, 1043–1053.

26 E. Martín-López, M. Darder, E. Ruiz-Hitzky and M. Nieto Sampedro, Agar-Based Bridges as Biocompatible Candidates to Provide Guide Cues in Spinal Cord Injury Repair, *Biomed. Eng. Mater.*, 2013, **23**, 405–421.

27 M. Milas, M. Rinaudo and B. Tinland, Polymer Bulletin The Viscosity Dependence on Concentration, Molecular Weight and Shear Rate of Xanthan Solutions, *Polym. Bull.*, 1985, **14**, 157–164.

28 M. R. Kasaai, J. Arul and G. R. Charlet, Intrinsic Viscosity-Molecular Weight Relationship for Chitosan, *J. Polym. Sci., Part B:Polym. Phys.*, 2000, **38**, 2591–2598.

29 G. Biagini, A. Bertani, R. Muzzarelli, A. Damadei, G. Dibenedetto, A. Belligolli, G. Riccotti, C. Zucchini and C. Rizzoli, Wound Management with *N*-carboxybutyl Chitosan, *Biomaterials*, 1991, **12**, 281–286.
30 T. Chandy and C. P. Sharma, Chitosan – as a Biomaterial, *Biomater., Artif. Cells, Artif. Organs*, 1990, **18**, 1–24.
31 J. E. Gough, P. Christian, C. A. Scotchford and I. A. Jones, Craniofacial Osteoblast Responses to Polycaprolactone Produced Using a Novel Boron Polymerisation Technique and Potassium Fluoride Post-Treatment, *Biomaterials*, 2003, **24**, 4905–4912.
32 J. E. Gough, P. Christian, J. Unsworth, M. P. Evans, C. A. Scotchford and I. A. Jones, Controlled Degradation and Macrophage Responses of a Fluoride-Treated Polycaprolactone, *J. Biomed. Mater. Res., Part A*, 2004, **69**, 17–25.
33 E. A. Elizalde-Peña, N. Flores-Ramirez, G. Luna-Barcenas, S. R. Vásquez-García, G. Arámbula-Villa, B. García-Gaitán, J. G. Rutiaga-Quiñones and J. González-Hernández, Synthesis and Characterization of Chitosan-*g*-Glycidyl Methacrylate with Methyl Methacrylate, *Eur. Polym. J.*, 2007, **43**, 3963–3969.
34 N. Flores-Ramírez, E. A. Elizalde-Peña, S. R. Vásquez-García, J. González-Hernández, A. Martinez-Ruvalcaba, I. C. Sanchez, G. Luna-Bárcenas and R. B. Gupta, Characterization and Degradation of Functionalized Chitosan with Glycidyl Methacrylate, *J. Biomater. Sci., Polym. Ed.*, 2005, **16**, 473–488.
35 A. Pawlak and M. Mucha, Thermogravimetric and FTIR Studies of Chitosan Blends, *Thermochim. Acta*, 2003, **396**, 153–166.
36 A. Pawlak and M. Mucha, Erratum: Thermogravimetric and FTIR Studies of Chitosan Blends [*Thermochimica Acta*, 2003, **396**, p. 153–166], *Thermochim. Acta*, 2004, **409**, 95–97.
37 E. A. Elizalde-Peña, D. G. Zarate-Triviño, S. M. Nuño-Donlucas, L. Medina-Torres, J. E. Gough, I. C. Sanchez, F. Villaseñor and G. Luna-Barcenas, Synthesis and Characterization of a Hybrid (Chitosan-*g*-Glycidyl Methacrylate)-Xanthan Hydrogel, *J. Biomater. Sci., Polym. Ed.*, 2013, **24**, 1426–1442.
38 D. Lien-Vien, N. B. Colthup, W. G. Fateley and J. G. Grasselli, *The Handbook of Infrared and Raman Characteristic Frequencies of Organic Molecules*, 1991.
39 M. Badertscher, P. Bühlmann and E. Pretsch, Structure Determination of Organic Compounds, *Tables of Spectral Data*, 2009.
40 Z. Sheikh, P. J. Brooks, O. Barzilay, N. Fine and M. Glogauer, Macrophages, Foreign Body Giant Cells and Their Response to Implantable Biomaterials, *Materials*, 2015, **8**, 5671–5701.
41 B. M. Gumbiner, Cell Adhesion: Review The Molecular Basis of Tissue Architecture and Morphogenesis, *Cell*, 1996, **84**, 345–357.
42 A. Przekora, The Summary of the Most Important Cell-Biomaterial Interactions That Need to Be Considered during *in Vitro* Biocompatibility Testing of Bone Scaffolds for Tissue Engineering Applications, *Mater. Sci. Eng., C*, 2019, **97**, 1036–1051.
43 A. E. Aguiar, M. de O. Silva, A. C. D. Rodas and C. A. Bertran, Mineralized layered films of xanthan and chitosan stabilized by polysaccharide interactions: a promising material for bone tissue repair, *Carbohydr. Polym.*, 2019, **207**, 480–491.
44 T. L. Hwang, I. A. Aljuffali, C. F. Lin, Y. T. Chang and J. Y. Fang, Cationic additives in nanosystems activate cytotoxicity and inflammatory response of human neutrophils: lipid nanoparticles *versus* polymeric nanoparticles, *Int. J. Nanomed.*, 2015, **10**, 371–385.
45 A. M. Rios, A. S. Medina, J. M. Irache, A. L. M. López, I. A. R. Espejel and J. M. C. Bravo, Toxicity evaluation of thermosensitive nanogels in an *in vivo* model, *Revista de Ciencias Tecnológicas*, 2022, **5**, e236.
46 K. Trescher, N. Scharnagl, K. Kratz, T. Roch, A. Lendlein and F. Jung, Adherence and viability of primary human keratinocytes and primary human dermal fibroblasts on acrylonitrile-based copolymers with different concentrations of positively charged functional groups, *Clin. Hemorheol. Microcirc.*, 2012, **52**, 391–401.
47 K. A. Bush, P. F. Driscoll, E. R. Soto, C. R. Lambert, W. G. McGimpsey and G. D. Pins, Designing tailored biomaterial surfaces to direct keratinocyte morphology, attachment, and differentiation, *J. Biomed. Mater. Res., Part A*, 2009, **90**, 999–1009.
48 J. Feng, L. Zhao and Q. Yu, Receptor-Mediated Stimulatory Effect of Oligochitosan in Macrophages, *Biochem. Biophys. Res. Commun.*, 2004, **317**, 414–420.
49 T. Mori, Y. Irie, S. Nishimura, S. Tokura, M. Matsuura, M. Okumura, T. Kadosawa and T. Fujinaga, Endothelial Cell Re-sponses to Chitin and Its Derivatives, *J. Biomed. Mater. Res.*, 1998, **43**, 469–472.
50 F. Chellat, A. Grandjean-Laquerriere, R. le Naour, J. Fernandes, L. Yahia, M. Guenounou and D. Laurent-Maquin, Metallo-proteinase, and Cytokine Production by THP-1 Macrophages Following Exposure to Chitosan-DNA Nanoparticles, *Biomaterials*, 2005, **26**, 961–970.
51 K. H. Biswas, Molecular Mobility-Mediated Regulation of E-Cadherin Adhesion, *Trends Biochem. Sci.*, 2020, **45**, 163–173.
52 E. Ruoslahti, Fibronectin in Cell Adhesion and Invasion, *Cancer Metastasis Rev.*, 1984, **3**, 43–51.
53 L. Parisi, A. Toffoli, B. Ghezzi, B. Mozzoni, S. Lumetti and G. M. Macaluso, A Glance on the Role of Fibronectin in Controlling Cell Response at Biomaterial Interface, *Jpn. Dent. Sci. Rev.*, 2020, **56**, 50–55.
54 B. L. Patton, J. H. Miner, A. Y. Chiu and J. R. Sanes, Distribution and Function of Laminins in the Neuromuscular System of Developing, Adult, and Mutant Mice, *J. Cell Biol.*, 1997, **139**, 1507–1521.
55 M. Paulsson, The Role of Laminin in Attachment, Growth, and Differentiation of Cultured Cells: A Brief Review, *Cytotechnology*, 1992, **9**, 99–106.
56 A. E. Haggerty, M. R. Bening, G. Pherribo, E. A. Dauer and M. Oudega, Laminin Polymer Treatment Accelerates Repair of the Crushed Peripheral Nerve in Adult Rats, *Acta Biomater.*, 2019, **86**, 185–193.
57 A. B. Reynolds and R. H. Carnahan, Regulation of Cadherin Stability and Turnover by P120ctn: Implications in Disease and Cancer, *Semin. Cell Dev. Biol.*, 2004, **15**, 657–663.

58 J. W. Rick, A. Chandra, C. Dalle Ore, A. T. Nguyen, G. Yagnik and M. K. Aghi, Fibronectin in Malignancy: Cancer-Specific Alterations, Protumoral Effects, and Therapeutic Implications, *Semin. Oncol.*, 2019, **46**, 284–290.

59 T. C. Lin, C. H. Yang, L. H. Cheng, W. T. Chang, Y. R. Lin and H. C. Cheng, Fibronectin in Cancer: Friend or Foe, *Cells*, 2020, **9**, 27.

60 P. Barraza-Flores, C. R. Bates, A. Oliveira-Santos and D. J. Burkin, Laminin and Integrin in LAMA2-Related Congenital Muscular Dystrophy: From Disease to Therapeutics, *Front. Mol. Neurosci.*, 2020, **13**, 1.

61 P. D. Yurchenco, K. K. McKee, J. R. Reinhard and M. A. Rüegg, Laminin-Deficient Muscular Dystrophy: Molecular Pathogenesis and Structural Repair Strategies, *Matrix Biol.*, 2018, **71–72**, 174–187.

62 E. A. Elizalde-Peña, I. A. Quintero-Ortega, D. G. Zárate-Triviño, A. Nuño-Licona, J. Gough, I. C. Sanchez, D. I. Medina and G. Luna-Barcenas, (Chitosan-*g*-Glycidyl Methacrylate)-Xanthan Hydrogel Implant in Wistar Rats for Spinal Cord Regeneration, *Mater. Sci. Eng., C*, 2017, **78**, 892–900.

63 H. A. López-Muñoz, M. Lopez-Romero, M. A. Franco-Molina, A. Manzano-Ramirez, C. Velasquillo, B. L. España-Sanchez, A. L. Martinez-Hernandez, H. Vergara-Castañeda, A. Giraldo-Betancur and S. Favela, Chitosan-*G*-Glycidyl Methacry-late/Au Nanocomposites Promote Accelerated Skin Wound Healing, *Pharmaceutics*, 2022, **14**, 1855.

64 W. Xue, W. Shi, Y. Kong, M. Kuss and B. Duan, Anisotropic Scaffolds for Peripheral Nerve and Spinal Cord Regeneration, *Bioact. Mater.*, 2021, **6**, 4141–4160.

65 S. Wu, T. Dong, Y. Li, M. Sun, Y. Qi, J. Liu, M. A. Kuss, S. Chen and B. Duan, State-of-the-Art Review of Advanced Electrospun Nanofiber Yarn-Based Textiles for Biomedical Applications, *Appl. Mater. Today*, 2022, **27**, 101473.

66 J. Liu, T. Li, H. Zhang, W. Zhao, L. Qu, S. Chen and S. Wu, Electrospun Strong, Bioactive, and Bioabsorbable Silk Fibroin/Poly(L-Lactic-Acid) Nanoyarns for Constructing Advanced Nanotextile Tissue Scaffolds, *Mater. Today Bio*, 2022, **14**, 100243.

67 Y. Li, T. Dong, Z. Li, S. Ni, F. Zhou, O. A. Alimi, S. Chen, B. Duan, M. Kuss and S. Wu, Review of Advances in Electro-spinning-Based Strategies for Spinal Cord Regeneration, *Mater. Today Chem.*, 2022, **24**, 100944.